

Revisiting the shape of pulsar beams

D. Mitra and A. A. Deshpande

Raman Research Institute, C. V. Raman Avenue, Bangalore - 560080, India
email:dmitra@rri.ernet.in, desh@rri.ernet.in

Received ? / Accepted ?

Abstract. Characterizing the shape and evolution of pulsar radio emission beams is important for understanding the observed emission. The various attempts by earlier workers investigating beam shapes have resulted in widely different conclusions. Using a carefully selected subset of the recently published multifrequency polarimetry observations of 300 radio pulsars (Gould & Lyne, 1998), we attempt to model the shape of pulsar beams. Assuming that the beam shape is elliptical, in general, and that it may depend on the angle between the rotation and the magnetic axes, we seek a consistent model where we also solve for the dependence of the beam size on frequency. From the six-frequency data on conal triple and multiple component profiles, we show that a) the pulsar emission beams follow a *nested cone* structure with at least *three distinct cones*, although only one or more of the cones may be active in a given pulsar; b) each emission cone is illuminated in the form of an annular ring of width typically about 20% of the cone radius.

Although some slight preference is evident for a model where the beam is circular for an aligned rotator & latitudinally compressed for an orthogonal rotator, the possibility that the beam shape is circular at all inclinations is found to be equally consistent with the data. While the overall size scales as $P^{-0.5}$ (where P is the pulsar period) as expected from the notion of dipolar open field lines, we see no evidence in support of the beam shape evolution with pulsar period.

Key words: pulsars:general–emission mechanism

1. Introduction

Most widely accepted emission models assume that pulsar radiation is emitted over a (hollow) cone centered around the magnetic dipole axis. The observed emission is generally highly linearly polarized with a systematic rotation of

the position angle across the pulse profile. This behaviour, following Radhakrishnan & Cooke (1969), is interpreted in terms of the radiation being along the cone of the dipolar open field-lines emerging from the polar cap, and the plane of the linear polarization is that containing the field line associated with the emission received at a given instant. During each rotation of the star, the emission beam crosses the observers line-of-sight resulting in a pulse of emission. The observed pulse profile thus corresponds to a *thin* cut across the beam at a fixed rotational latitude. The information on the beam shape as a function of latitude, although generally not measurable directly, may be forthcoming from observations at widely separated frequencies, as emission at different frequencies is believed to originate at different heights from the star leading to changes in beam size. For this, the dependence of the radiation frequency on the height, the so called *radius-to-frequency mapping*, should be known a priori. Alternatively, it is possible to use the data on an ensemble of pulsars sampling a range of impact parameters. However, it is important that all the pulsars in the sample form a homogeneous set in terms of the profile types etc. Several attempts to model the pulsar beam have used the latter approach. Based on their study, Narayan and Vivekanand (1983) concluded that the beam is elongated in the latitude. Lyne & Manchester (1988), on the other hand, have argued that the beam is essentially circular (see also Gil & Han 1996, Arendt & Eilek 1998). Based on the dipole geometry of the cone of open field-lines, Biggs (1990) found that the beam shape is a function of the angle (α) between the rotation and the magnetic axes. The reasons that all these analyses predict different results could be manifold. For example, Narayan & Vivekanand used a data set consisting of only 16 pulsars and assessed the beam axial ratio on the basis of the total change in the position angle of the linear polarization across the pulse profile. Apart from poor statistics, their analysis suffered from the large uncertainties in the polarization measurements available then. Lyne & Manchester (1988) used a much larger data set in comparison and examined the distribution of normalized impact parameter $\beta_n \equiv \beta_{90}/\rho_{90}$, where β_{90} & ρ_{90} are the impact angle and the beam radius computed for $\alpha = 90^\circ$. Based on

their observation that the distribution of β_n is ‘essentially uniform’, they concluded that the beams are circular in shape. The apparent deficit at large β_n is attributed to a luminosity bias. It is worth noting that the deficit is seen despite the fact that β_n overestimates the *true* β/ρ (given that they disregarded the sign of β), this is particularly so at large β values.

Biggs (1990) used the same data set as well as the β_n distribution as used by Lyne and Manchester (1988), but drew attention to a ‘peak’ in the distribution at low β_n . The shapes of the polar cap defined by the region of open field lines, as derived by Biggs, show that the beam is circular for an aligned rotator, but undergoes compression along the latitudinal direction with increasing inclination α .

In this paper, we address this question within the basic framework advanced by Rankin (1993a) which, at the least, is qualitatively different from that of Lyne & Manchester (1988). The classification scheme (Rankin, 1983a), based on the phenomenology of pulse profiles, polarization and other fluctuation properties etc., provides a sound basis for explicit distinction between the core and the conal components, with each of them following a predictable geometry (see also Oster & Sieber 1976; Gil & Krawczyk 1996 for *conal beams*). Lyne & Manchester (1988), on the other hand, prefer to interpret the observed variety in pulse shape and other properties as a result of patchy illumination, rather than any particular pattern within the radiation cone. The observed differences in the properties of pulse components are then to be understood as gradual changes as a function of the distance from the center of the basic emission cone. Their analysis thus naturally disregards the possible existence of conal features.

Assuming the possibly confined ‘conal-component’ geometry and by accounting for all the relevant geometrical effects, we re-examine the shape of pulsar beams and their frequency dependence. Recently published multifrequency polarization data, at six frequencies in the range between 234-1642 MHz (Gould & Lyne, 1998), has made this investigation possible.

2. Data set

For the present investigation requiring reliable estimates of α & β , we use the data set comprised of only those pulsars whose pulse profiles are identified as ‘triple’ (**T**) or ‘multiple’ (**M**), as classified by Rankin (1993a, 1993b). The reason for the choice is that the **T** and **M** pulsars show a core component in addition to the conal components, so that a reliable estimation of the angle (α) between the rotation axis and the magnetic axis is possible, using Rankin’s (1990) method. In this method, the ratio of the observed core-width to the limiting width ($2.45^\circ P^{-0.5}$) is interpreted as the geometric factor $1/\sin(\alpha)$, providing by far the most reliable estimates of α . For the conal doubles and conal singles, devoid of any core component, the

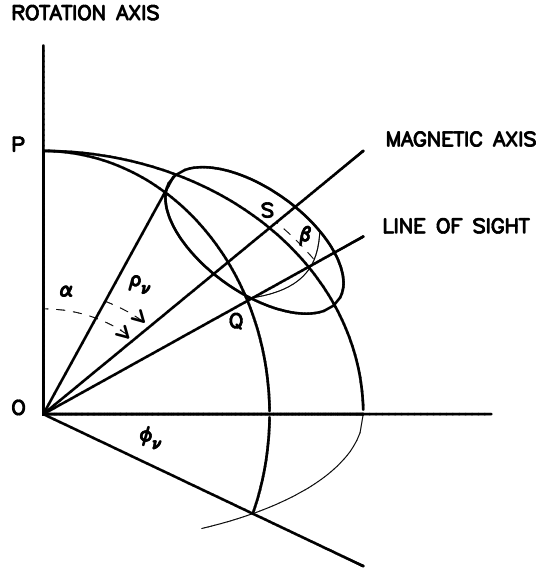


Fig. 1. Schematic representation showing the geometry of the pulsar emission region.

estimates of α are less reliable. The core singles are naturally excluded from this analysis of the conal emission geometry. For each pulsar in our selected sample, we define the conal width as the separation between the peaks of the outermost conal components. It is important to note that the nominally ‘central’ core component, which is argued to originate closer to the stellar surface, may not necessarily be along the cone axis. Such a possibility is clearly reflected in many pulse profiles where the core component is displaced from the ‘center’ definable from the conal components. Hence, the location of the core component is disregarded in our estimation of the conal separation. Columns 1 and 2 of table 1 list the name and profile type of these pulsars. Columns 3 to 8 list the calculated widths of the pulsars at frequencies 234, 408, 610, 925, 1400, and 1642 MHz respectively. Column 9 gives the pulsar period in seconds. Columns 10 and 11 list the α and β values of the pulsars taken from Rankin (1993b).

Rankin (1990) has estimated the inclination angle α using the relation, $\sin(\alpha) = 2.45^\circ P^{-0.5}/W_{\text{core}}$, where W_{core} is the half-power width of the core component (at a reference frequency 1 GHz) and the period P is in seconds. The impact angle β has been estimated based on the rotating vector model of Radhakrishnan & Cooke (1969), using the relation $\sin(\beta) = (d\chi/d\phi)_{\text{max}}/\sin(\alpha)$, where $(d\chi/d\phi)_{\text{max}}$ is the maximum rate of change of the polarization angle χ with respect to the longitude ϕ .

In the following analysis, we treat the different frequency measurements on a given pulsar as ‘independent’ inputs much the same way as the data on different pulsars, since the pulsar beam size is expected to evolve with frequency. Thus, at different frequencies one obtains independent cuts (at different β/ρ) across the beam, though β remains constant for a given pulsar. This increases the

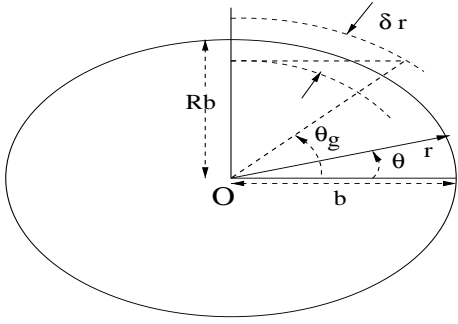


Fig. 2. Schematic representation of an elliptic pulsar beam of axial ratio R with the longitudinal and the latitudinal axis as b and Rb respectively. δr is the width of the emission beam cone. See text for discussion on the connection between the ‘gap-angle’ θ_g and $\delta r/r$.

number of independent constraints by a usefully large factor. In fact, we would like to contrast this approach with the one where, for each pulsar, one obtains a best fit frequency dependence of the observed widths and then uses the data to obtain the width at a chosen reference frequency. The latter approach fails to take into account the dependence of the observed widths on β/ρ that is inherent for any non-rectangular shape of the beam.

3. A direct test for the shape of beams

The Fig 1 is a schematic diagram illustrating the geometry of pulsar emission cone. The emission cone, with half-opening angle ρ_ν , sweeps across the observers line-of-sight with an impact parameter (distance of closest approach to the magnetic axis) β . The spherical triangle PQS (refer to Fig. 1) relates the angles α , β and the profile half-width ϕ_ν to the beam radius ρ_ν by the following relation (Gil, Gronkowski & Rudnicki 1984),

$$\sin^2(\rho_\nu/2) = \sin^2(\phi_\nu/2) \sin(\alpha) \sin(\alpha + \beta) + \sin^2(\beta/2) \quad (1)$$

The subscript ν in ρ_ν and ϕ_ν denotes that these quantities depend on frequency ν . This equation assumes that the cone is circular, in which case ρ_ν becomes independent of β .

In reality, the beam may not be circular, but rather elliptical with, say, R the axial ratio and b the longitudinal semi-axis of the ellipse as shown in Fig. 2. It is easy to see that the length of the radius vector r depends on the angle θ (with the longitudinal axis) when R is not equal to 1. The variation of r as a function of θ for three different R values (namely 1, 1.5 and 0.5) are shown as examples in Fig. 3. The ρ_ν , determined assuming that the cone shape is circular (as in Rankin 1993b) is indeed a measure of the radius vector r , once the period and frequency dependences are corrected for. Such data on (r, θ) spanning a wide enough range in θ can therefore be examined to seek a consistent value of the axial-ratio R . However, if R is a function of α , as suggested by Biggs (1990), then the

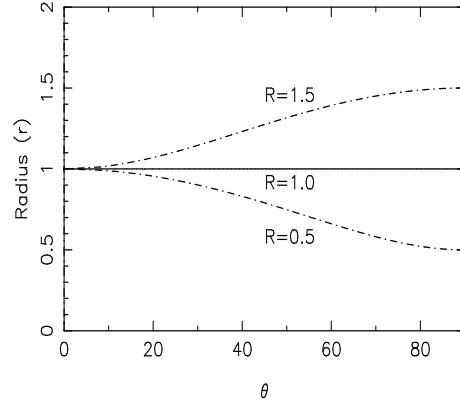


Fig. 3. The above curves illustrate the normalized variation of r with θ (refer to figure 2) with three different values of R .

(r, θ) samples would show a spread bounded by the curves corresponding to the maximum and minimum values of R .

Such an examination of the present data suggests a spread below the line for $R = 1$, indicating that the beam deviates from circularity and that the spread could be due to the α dependence of R . However, this deviation from circularity is not very significant. We discuss this in detail later in section 5.

We have also examined the ρ_ν values obtained by Rankin (1993b) through such a test. However, no significant deviation from circular beams was evident. We became aware of a similar study by C.-I. Björnsson (1998), also with a similar conclusion. We note that the only difference between our estimates of ρ_ν and those of Rankin is in the definition of the conal widths. Rankin defines the width as the distance between the outer half-power points (rather than the peaks) of the two conal outriders, and the widths were then ‘interpolated’ to a reference frequency of 1 GHz. Such estimates are prone to errors due to mode changes, differing component shapes etc., and to the effects of dispersion & scattering (some of which she attempted to accommodate). We measure the widths as the peak-to-peak separations of the outer conal components, which are less sensitive to the sources of error mentioned above. We have also confirmed (in the PSRs 0301+19, 0525+21, 0751+32, 1133+16, 1737+13, 2122+13 and 2210+29 using the data from Blaskiewicz et al. 1991) that the ‘peaks’ of the conal components are symmetrically placed with respect to the “zero-longitude” (associated with the maximum rate of change of the position angle), which is not always true for the outer half-power points.

Table 1. The table lists the pulsar name and the widths measured at 6 different frequencies from the observations of Gould & Lyne (1998). In several cases the widths could not be estimated due either to poor quality profiles or to absence of data. The α , β values are taken from Rankin (1990, 1993b). *LM* indicates that the β value (for PSR 0656+14 and 1914+09) is taken from Lyne & Manchester (1988).

Pulsar Bname	Profile Class	Width in deg						Period (sec)	α (deg)	β (deg)
		W_{234}	W_{408}	W_{610}	W_{925}	W_{1400}	W_{1642}			
0329+54	T	25.4	23.3	21.8	21.8	21.2	20.7	0.714518	30	2.1
0450-18	T	16.6	14.5	13.5	12.9	12.4	11.9	0.548937	24	4
0450+55	T	27.3	20.7	20.7	24.6	22.0	22.0	0.340729	32	3.3
0656+14	T	27.9	21.7	17.8	25.5	20.1	17.8	0.384885	30	8.2 (LM)
0919+06	T	18.1	16.5	14.6	11.5	10	8.4	0.430619	48	4.8
1508+55	T	-	12.0	8.57	11.6	10.9	10.5	0.739681	45	-2.7
1541+09	T	126.5	107.8	105.4	96.0	91.4	84.3	0.748448	5	0.0
1738-08	T	-	14.6	13.7	13.6	12.6	12.1	2.043082	26	1.7
1818-04	T	-	10.7	8.2	9.20	8.8	8.5	0.598072	65	3.5
1821+05	T	36.2	32.1	29.4	29.4	26.6	26.6	0.752906	32	1.7
1911+13	T	-	12.3	10.7	12.0	11.6	11.0	0.521472	52	1.9
1914+09	T	-	10.9	12.6	8.9	8.5	8.1	0.270254	52	7.3 (LM)
1917+00	T	-	8.3	8.1	8.0	7.2	6.7	1.272255	81	1.3
1918+19	T	-	49.1	42.7	41.3	41.3	38.7	0.821034	12	-4.6
1919+14	T	-	22.3	20.7	18.7	19.7	17.1	0.618179	26	-6.4
1919+21	T	-	7.17	6.7	8.2	7.6	7.4	1.337301	45	-3.7
1920+21	T	-	15.1	10.1	14.4	14.0	13.2	1.077919	44	1.1
1944+17	T	-	25.2	23.3	33.0	33.0	31.0	0.440618	19	6.1
2045-16	T	-	12.9	12.3	11.6	11.0	10.7	1.961566	36	-1.1
2111+46	T	69.8	63.3	59.4	55.6	53.0	49.1	1.014684	9	1.4
2224+65	T	39.9	35.0	31.1	31.1	31.1	31.1	0.682537	16	3.4
2319+60	T	21.8	18.7	17.1	15.0	13.5	13.5	2.256487	18	2.2
1804-08	M/T	-	28.5	12.9	16.2	15.5	14.2	0.163727	63	5.1
1910+20	M/T	-	12.8	11.5	11.2	10.8	-	2.232963	29	1.5
1952+29	M/T	-	22.7	21.6	22.2	21.0	19.2	0.426676	30	-7.2
2020+28	M/T	12.9	10.9	10.1	10.1	9.74	9.3	0.343401	72	3.6
0138+59	M	25.8	20	23.2	20.6	18.7	17.4	1.222948	20	2.2
0402+61	M	14.2	14.6	10.7	10.3	10	9.6	0.594573	83	2.2
0523+11	M	-	12.4	10.8	12.0	11.6	10.8	0.354437	78	5.9
0621-04	M	18.5	21.2	18.4	18.0	17.5	-	1.039076	32	0.0
1039-19	M	15.4	-	11.5	10.7	10	9.6	1.386368	31	1.7
1237+25	M	10.0	10.3	10.0	9.3	9.0	10.0	1.382449	53	0.0
1737+13	M	-	17.4	17.0	16.1	15.2	13.8	0.803049	41	1.9
1831-04	M	95.3	97.6	95.3	96.2	93.0	93.0	0.290106	10	2.0
1857-26	M	-	32.5	29.4	26.3	25.5	24.8	0.612209	25	2.2
1905+39	M	-	15.1	13.7	13.1	12.6	11.7	1.235757	33	2.1
2003-08	M	55.6	40.0	38.7	33.6	32.3	31.0	0.580871	13	3.3

4. The model of the pulsar beam

We model the pulsar beam shape as elliptical in general and express it analytically as,

$$\frac{\sin^2(\phi_\nu/2) \sin(\alpha) \sin(\alpha + \beta)}{\sin^2(\rho_\nu/2)} + \frac{\sin^2(\beta/2)}{\sin^2(R\rho_\nu/2)} = 1 \quad (2)$$

While α , β and ϕ_ν can be estimated, directly or indirectly, from observations, R and ρ_ν are the two parameters which in turn define the beam shape and size— and the available data set of **T** and **M**-profiles is expected to sample most of the $|\beta/\rho_\nu|$ range (0–1) with reasonable uniformity. The

implicit assumption in this statistical approach is that a common description for R & ρ_ν is valid for all pulsars. The common description should, however, account for relevant dependences on quantities, such as frequency, period, α , etc. properly.

4.1. Frequency dependence of ρ_ν

The radio emission at different frequencies is expected to originate at different altitudes above the stellar surface, with the higher frequency radiation associated with regions of lower altitude. This phenomenon known as *radius-to-frequency mapping*, finds overwhelming support from observations. Thorsett (1991) has suggested an empirical relation for the observed pulse width as a function of frequency, which seems to provide adequate description of the observed behaviour. We adopt a similar relation for the frequency evolution of the beam radius ρ_ν as follows

$$\rho_\nu = \hat{\rho}(1 + K\nu^{-\zeta}), \quad (3)$$

where $\hat{\rho}$ is the value of ρ_ν at infinite frequency, ζ the spectral index, and K a constant. Note that both ζ & K are expected to have positive values, so that the minimum value of ρ_ν is $\hat{\rho}$, which should correspond to the angular size of the polar cap.

4.2. Period dependence on ρ_ν

Rankin (1993a) has demonstrated (see also Gil, Kijak & Seiradakis 1993; Kramer et al. 1994) that the beam radius $\hat{\rho}$ varies as $P^{-0.5}$ (where P is the period of the pulsar), a result which is in excellent agreement with that expected from a dipole geometry (Gil 1981). Eq 3 thus takes the form

$$\rho_\nu = \rho_o(1 + K\nu^{-\zeta})P^{-0.5}, \quad (4)$$

where ρ_o is the minimum beam radius for $P = 1$ sec.

4.3. Functional dependence of R on α

Biggs (1990) has suggested that R should be a function of α , such that the beam shape is circular for $\alpha = 0$ and is increasingly compressed in the latitudinal direction as α increases to 90° . We therefore model the functional dependence of R on α as $R = R_o\tau$, where R_o is the axial ratio of the beam at $\alpha = 0$, and τ is a function of α . According to Biggs (1990), $R_o = 1$ and τ is given by

$$\tau(\alpha) = 1 - K_1 \times 10^{-4}\alpha - K_2 \times 10^{-5}\alpha^2, \quad (5)$$

where K_1 , K_2 are constants and α is in degrees. Biggs finds that K_1 and K_2 are 3.3 and 4.4, respectively. We, however, treat $K_{1,2}$ as free parameters in our model.

4.4. The number of hollow cones

Based on the study of conal components, Rankin (1993a) has argued for two nested hollow cones of emission—namely, the outer and the inner cone. Assuming the beams to be circular in shape, opening half angles of the two cones at 1 GHz were found to be 4.3° and 5.7° , respectively.

During our preliminary examination of the present sample, we noticed a need to allow for three cones of emission. To incorporate this feature in our model, we introduce two ratios, $r1 < 1$ and $r2 > 1$, to define the size scaling of the inner-most and the outer-most cone, respectively, with reference to a ‘middle’ cone, for which the detailed shape is defined.

Using the model here defined, we need to solve for R_o , ζ , K , ρ_o , K_1 , K_2 , $r1$ and $r2$ in this three-conal-ring model. The parameter set thus represents an ‘average’ description of the beam.

5. Results and Discussion

An optimized grid search was performed for suitable ranges of the parameter values and in fine enough steps. For ζ , the search range allowed for both +ve and -ve values. By definition, $r_1 \leq 1$ and $r_2 \geq 1$. The best fit was obtained by minimizing the standard deviation σ_o defined by

$$\sigma_o = \sqrt{\frac{\sum_{i=1}^n D_i^2}{N_{dof}}} \times \frac{180^\circ}{\pi}, \quad (6)$$

where D_i is the deviation of the i^{th} data point from the nearest conal ring in the model and N_{dof} denotes the degrees of freedom. The factor $180/\pi$ gives σ_o in units of degrees under the small-angle approximation. Table 2 lists the parameter values which correspond to the best fit for the entire sample set. With these values, the eq. 4 can now be rewritten as

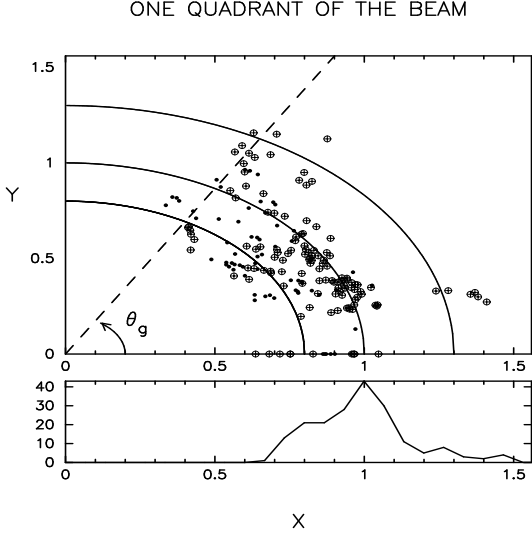
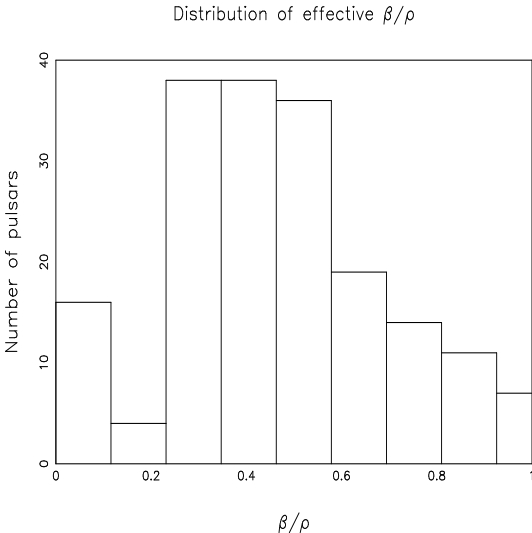
$$\rho_\nu = 4.8^\circ(1 + 66 \nu_{\text{MHz}}^{-1})P^{-0.5}, \quad (7)$$

where ρ_ν is in degrees. This average description for the ‘middle’ cone applies also to the other two cones when ρ_ν is scaled by the ratio $r1 = 0.8$ or $r2 = 1.3$ (for the inner and the outermost, respectively). Fig 4 shows the data (plotted to a common scale) for one quadrant of the beam and the three solid curves corresponding to the best fit cones. The points in the figure, though corresponding to different pulsars and frequencies, are translated to a common reference scale appropriate for $P = 1$ sec, $\alpha = 0$ and $\nu = \infty$.

We have assumed the period dependence of ρ_ν as $P^{-0.5}$, whereas Lyne and Manchester (1988) found a dependence of $P^{-\frac{1}{3}}$. We have examined the latter possibility and found that the difference in the standard deviation is at the level of $2.5\text{-}3\sigma$ and we cannot rule out the $P^{-\frac{1}{3}}$ law

Table 2. The best-fit model parameters for the shape of conal beams. The error bars correspond to a 1σ uncertainty.

Model parameters							
R_o	ρ_o (deg)	K	ζ	$r1$	$r2$	K_1 (deg $^{-1}$)	K_2 (deg $^{-2}$)
$0.91 \pm_{0.1}^{0.2}$	4.8 ± 0.3	66 ± 10	1 ± 0.1	0.8 ± 0.03	1.3 ± 0.03	7.2 ± 0.2	4.4 ± 0.3

**Fig. 4.** Distribution of the (x,y) locations of the conal components on a common scale. The three solid lines indicate the three emission cones in the quadrant shown. The circles with crosses refers to pulsars with α values less than 45° and the filled circles with α greater than 45° .**Fig. 5.** Histogram of the distribution of effective $\frac{\beta}{\rho}$.

with confidence. We have also checked for the dependence of R on α by using 3 sub-sets, each of range 30° in α . The best fit values for R in the different α segments are $1 \pm_{0.2}^{0.4}$, $0.8 \pm_{0.2}^{0.4}$ & $0.5 \pm_{0.2}^{0.4}$ for α ranges $0^\circ - 30^\circ$, $30^\circ - 60^\circ$ & $60^\circ - 90^\circ$, respectively. This dependence of R_o on α , even if it were significant, is quite consistent with our val-

ues of K_1 , K_2 (Table 2) as well as with the results of Biggs (1990). However, given the uncertainties in the R estimates for the three ranges, it is not possible presently to rule out a dependence of R on α . Indeed, this part of the goodness-of-fit is negligible, σ_o (the standard deviation) is 0.18° when K_1 and $K_2 \neq 0$ and 0.2° when $K_1, K_2 = 0$. Earlier Narayan & Vivekanand (1983) had argued that R is a function of the pulsar period. To assess this claim, our sample was divided into three period ranges and the corresponding R estimates compared. However, no period dependence was evident and it was possible to rule out such a dependence with high confidence.

The number and thickness of conal rings: As already noted and can be seen in Figure 4, we do see evidence for a possible cone outside the two cones discussed by Rankin (1993a). Also, presence of a ‘further inner’ cone has been suggested by Rankin & Rathnasree (1997) in the case of PSR 1929+10. The pulsars suggestive of this outer cone (refer Figure 4) are PSRs 0656+14, 1821+05, 1944+17 and 1952+29 (at frequencies 234 MHz and higher). We have examined the possibility that these cases really belong to the central-cone, but are well outside of it due to an error in the assumed values of α . We rule out the possibility as the implied error in α turns out to be too high to be likely. It is important to point out that a noisy sample like the present one would appear increasingly consistent, judging by the best-fit criterion, with models that include more cones. The question, therefore is whether we can constrain the number of cones by some independent method. In this context, we wish to discuss *the noticeable deficit of points at high β/ρ_o* . Since the deficit reflects the absence of conal singles and conal doubles in our data set, the size of the related ‘gap’ at large θ values, can be used to estimate the possible thickness of the conal rings. The absence of points at $\theta \gtrsim 60^\circ$ (Figure 4) suggests that the conal rings are rather thin, since a radial thickness δr comparable to the ring radius would imply a wider gap in θ . To quantify this, we write the following relation,

$$\delta r = 2r \frac{(1 - \sin \theta_g)}{(1 + \sin \theta_g)}, \quad (8)$$

where θ_g is the θ at the start of the gap (as illustrated in Fig. 2). With $\theta_g \sim 60^\circ$, $\delta r/r$ would be about 20%. The presence of more than one distinguishable peak in the distribution of beam radii (shown in the bottom panel of Fig. 4) clearly indicates that the conal separation is larger than the cone width. This combined with our cone-width estimate suggests the number of cones is 3 (for the present

range of radii), providing an independent support for our model. This picture is consistent with the estimates by Gil & Krawczyk (1997) and Gil & Cheng (1999).

Component separation vs. frequency: It is interesting to note that for certain pulsars the cone associated with the emission seems to change with frequency. For example, the conal emission in PSR 1920+21 appears to have ‘switched’ at 610 MHz to the innermost cone while being associated with the central cone at other frequencies. Rankin (1983b), in a comprehensive study of the dependence of component separation with frequency, invokes deep ‘absorption’ features to explain the apparent anomalous reduction in the component separation in certain frequency ranges. We suggest that such anomalous reduction in the separations could be due to switching of the emission to an inner cone at some frequencies. Observations at finely spaced frequencies in the relevant ranges would be helpful to study this effect in detail. The other pulsars which show similar trends are PSRs 1804-08, 2003-08, 1944+17 and 1831-04. It should be noted that such switching is possibly reflected, also, in mode changes.

The deficit at low β/ρ_o : The absence of points near $\beta = 0$ is clearly noticeable in Fig. 4. Such a ‘gap’ is also apparent in the distribution of β/ρ_o plotted in Fig. 5. The gap was already noted by Lyne & Manchester (1988). They argued that it arises because the rapid position-angle swings (expected at small β ’s) are difficult to resolve due to intrinsic or instrumental smearing, leading to underestimation of the sweep-rates. With the improved quality of data now available, the intrinsic smearing is likely to be the dominant cause for this circumstance. There are a number of clear instances among the general population of pulsars where the polarization angle traverse near the central core component is distorted. PSR 1237+25 provides an extreme examples of such distortion, and Ramachandran & Deshpande (1997) report promising initial efforts to model its polarization-angle track as distorted by a low- γ core-beam. Another possibility for the low- β/ρ_o gap is that it could simply be a selection effect caused by less intense emission in the cone center than at intermediate traverses. If so, the low frequency turn-overs in the energy spectra of pulsars may at least be partly due to this, since at lower radio frequencies the β/ρ_o is relatively smaller.

The sources of uncertainties in the present analysis: The standard deviation σ_o corresponding to the best-fit model amounts to about 15% of the conal radius. This fractional deviation (comparable to the thickness of the cone) is too large to allow any more detailed description of the beam shape (such as dependence on α , for example). We find it useful to assess and quantify the sources of error, partly to help possible refinement for future investigations. The three data inputs to our analysis are α , β and ϕ_ν , while the basic observables are the maximum polarization-angle sweep rate and core width, apart from the conal separation measured. It is easy to see that the errors in the core-widths will affect directly both α and

β estimates. Over the range of θ s spanned by the present data set the errors in α are likely to dominate, since the x & y (in figure 4) are almost linearly proportional to $\sin(\alpha)$. Hence, the fractional deviation may be nearly equal to (or define the upper limit of) the fractional error in $\sin(\alpha)$ and therefore in the core-width estimates.

Rankin (1990, 1993b) notes that in several cases the apparent core-widths might suffer from ‘absorption’ and the widths might be underestimated if the effect is not properly accounted for. Also, in some cases, the widths were extrapolated to a reference frequency of 1 GHz using a $\nu^{-0.25}$ dependence. There have been several suggestions regarding the ‘appropriate’ frequency dependence which would give significantly different answers when used for width extrapolation. For example, if our best-fit dependence for conal width is used for the core-width extrapolation, the values would differ from Rankin’s estimates (through extrapolation) by as much as 15%, enough to explain the present deviation in some cases. Another possible source of error is the uncertainty in the sign of β (important only for the $\sin(\alpha + \beta)$ term in equation 2 and hence for small α). As Rankin points out, it is difficult to determine the sign unambiguously in most cases and hence the information is only available for a handful of pulsars.

Evidence in favour of ‘conal’ emission: The significant implication of the gap at $\theta \gtrsim 60^\circ$ (referred to earlier) deserves further discussion. If the ‘conal’ components were results of a merely patchy (random) illumination across the beam area, (as argued by Lyne & Manchester, 1988), then such a gap should not exist. If a single thick hollow cone were to be responsible for the conal components, a gap (corresponding to the conal-single types) would still be apparent but then it should be above a cut-off y value (refer figure 4) and not in an angular sector like that observed. On the other hand, if indeed the conal emission exists in the form of nested cones (as distinct from the core emission), then the shape of the gap is a natural consequence of our not including conal-single profiles in this analysis. This gap, therefore, should be treated as an important evidence for a pulsar beam form comprised, in general, of nested cones of emission.

6. Summary

Using the multifrequency pulse profiles of a large number of conal-triple and multiple pulsars we modelled the pulsar beam shape in an improved way. Our analysis benefits from the different frequency measurements being treated as independent samples, thus increasing the number of independent constrains. The main results are summarized below.

1) Our profile sample is consistent with a beam shape that is a function of α , circular at $\alpha = 0$ and increasingly compressed in the latitudinal direction as α increases, as suggested by Biggs (1990). However, the data is equally

consistent with the possibility that the beam is circular for all values of α .

2) We identify three nested cones of emission based on a normalized distribution of outer components. The observed gap ($\theta \gtrsim 60^\circ$) in the distribution independently suggests three cones in the form of annular rings whose widths are typically about 20% of the cone radii. We consider this circumstance as an important evidence for the nested-cone structure.

Any further significant progress in such modelling would necessarily need refined estimates of the observables, particularly the core-widths.

Acknowledgement

We thank V. Radhakrishnan, Rajaram Nityananda and Joanna Rankin for fruitful discussions and for several suggestions that have helped in improving the manuscript. We acknowledge Ashish Asgekar, D. Bhattacharya and R. Ramachandran for useful discussions and thank our referee, J. A. Gil, for critical comments and suggestions.

References

- Arendt, P. N. & Eilek, J. A., 1999, ApJ, preprint.
 Biggs, J. D., 1990, M.N.R.A.S, **245**, 514.
 Björnsson, C-I., 1998, A&A, **338**, 971.
 Blaskiewicz, M., Cordes, J. M. & Wasserman, I., 1991, ApJ, **370**, 643.
 Gil, J. A., 1981, Acta phys Polonicae, **B12**, 1081.
 Gil, J. A., Gronkowski, P. & Rudnicki, W., 1984, A&A, **132**, 312.
 Gil, J. A., & Cheng. K. S., 1999, preprint.
 Gil, J. A., & Han. J. L., 1996, ApJ, **458**, 265.
 Gil, J. A., Kijak, J. & Seiradakis, J. H., 1993, A&A, **272**, 268.
 Gil, J. A., Krawczyk. A., 1996, M.N.R.A.S, **280**, 143.
 Gil, J. A., Krawczyk. A., 1997, M.N.R.A.S., **285**, 561.
 Gould, M. & Lyne, A. G., 1998, M.N.R.A.S, **301**, 235.
 Kramer, M., Wielebinski, R., Jessner, A., Gil, J. A. & Seiradakis, J. H., 1994, A&A, **107**, 515.
 Lyne, A. G. & Manchester, R. N., 1988, M.N.R.A.S, **234**, 477.
 Narayan, R. & Vivekanand, M., 1983, Astron. Astrophysics, **122**, 45.
 Oster, L. & Sieber, W., 1976, ApJ, **210**, 220.
 Radhakrishnan, V. & Cooke, D. J., 1969, Ap. Letters, **3**, 225.
 Ramachandran, R. & Deshpande A. A., 1997, private communication
 Rankin, J. M., 1983a, ApJ, **274**, 333.
 Rankin, J. M., 1983b, ApJ, **274**, 359.
 Rankin, J. M., 1990, ApJ, **352**, 247.
 Rankin, J. M., 1993a, ApJ, **405**, 285.
 Rankin, J. M., 1993b, ApJS, **85**, 145.
 Rankin, J. M. & Rathnasree, N., 1997, JAA, **18**, 91.
 Thorsett, S., 1991, ApJ, **377**, 263.